INTERNATIONAL JOURNAL FOR NUMERICAL AND ANALYTICAL METHODS IN GEOMECHANICS, VOL. 20, 173–190 (1996)

NON-LINEAR FAULT BEHAVIOUR NEAR UNDERGROUND EXCAVATIONS — A BOUNDARY ELEMENT APPROACH

KEYVAN FOTOOHI* AND HANI S. MITRI†

Department of Mining and Metallurgical Engineering, McGill University, Montreal, Quebec, Canada H3A 2A7

SUMMARY

A boundary element model for stress/stability analysis of underground excavations in the vicinity of faults is presented. The boundary element formulation adopts the fictitious stress method for the simulation of excavation boundaries and the displacement discontinuity method for the representation of faults. The numerical model employs the Barton–Bandis non-linear joint model for the modelling of the fault behaviour and linear elastic behaviour for the rock. An incremental-iterative *in situ* stress relaxation algorithm is implemented for the non-linear analysis of the faults. Both deformation and peak strength models of Barton–Bandis are incorporated for modelling the mechanical behaviour of the fault. The non-linear deformation of fault considers the effects of coupling between shear and normal stresses and displacement, joint closure, joint separation, hardening followed by post-peak or residual behaviour. The peak strength model employs a mobilized non-linear shear strength envelope. The differences between linear and non-linear simulation of the fault models are discussed. A comparison of model predictions with the classical Mohr–Coulomb peak strength model with constant joint stiffness is presented. The numerical model is used for a case study of Canadian hard rock underground mine. The shear and normal displacements along the fault during four mining sequences with backfill simulation are presented and discussed.

KEY WORDS: stress/stability analysis; constitutive modelling; non-linear fault behaviour

INTRODUCTION

Constitutive modelling of rock discontinuities has been a subject of interest to researchers over the past 25 years. Goodman *et al.*[1] first introduced the terms normal stiffness (K_n) and shear stiffness (K_s) of a joint to define the rate of change of normal stress with respect to normal displacement and of shear stress with respect to shear displacement, respectively. Goodman[2] later showed that the relation between joint closure and normal stress can be a hyperbolic function with the maximum closure, V_{rm}, of the joint being less than its aperture thickness. The shear deformation versus shear stress relation was defined as linear elastic to peak followed by post-peak behaviour as shown in Figure 1. Goodman[2] also proposed that the variation of peak shear displacement and shear stiffness with changing normal stress can be simplified using one of two models. One model assumes that the shear stiffness and the slope of the post-peak region are independent of the normal stress (constant stiffness model). The second model assumes that the peak and residual shear displacement are constant (constant displacement model).

Fortin *et al.*[3,4] developed an algorithm based on interpolation of experimental data of direct shear test under constant normal stress. It allows for the prediction of normal stress, shear stress and closure all as functions of shear displacement along a discontinuity at a given normal stiffness. Saeb and Amadei[5] proposed a simple graphical method to predict the shear response of

*Postdoctoral Fellow
†Associate Professor

CCC 0363–9061/96/030173–18

Received 9 May 1994
Revised 18 August 1995

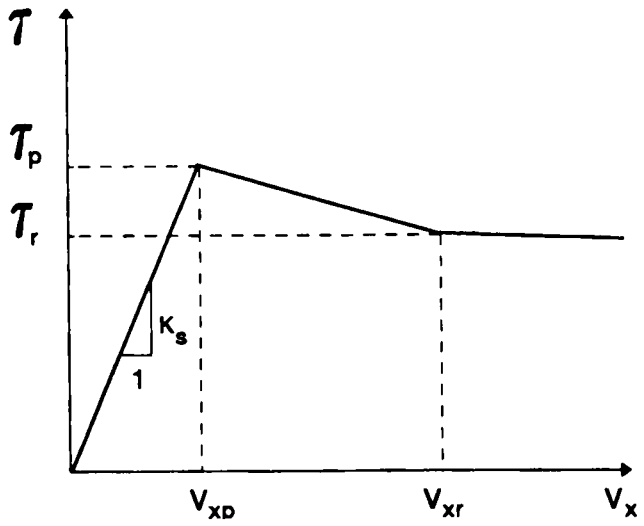

Figure 1. Shear stress–displacement deformation of a joint (after Reference 2)

a dilatant rock joint having constant or variable normal stiffness knowing its behaviour under constant normal stress. This method uses the curves of behaviour of an idealized joint under increasing normal stress (with zero shear stress) and its behaviour under increasing shear stress (with constant normal stress), which were also proposed by Goodman and Boyle.[6] Saeb and Amadei[7] later presented their graphical method in a mathematical form. The proposed method provides a tangent formulation for the deformability of a dilatant rock joint. The increments of shear and normal stress are related to the increments of shear and normal displacement through a 2×2 material tangent stiffness matrix.

BOUNDARY ELEMENT APPLICATION IN ROCK MATERIALS

Rock mechanics problems in mining engineering are distinguished from other engineering problems in the sense that they are often very large in scale and deal with infinite, inhomogeneous and discontinuous material domain. In the boundary Element Method (BEM), only the boundary of the problem requires discretization. This feature makes the BEM very suitable for the mining problems. The first references to the application of the BEM to mining engineering problems was made by Salamon[8–11] who used the so-called constant elements. His work was followed by Starfield and Crouch[12] who generalized it and used it to solve different types of problems, and by Diest[13] who used the technique to analyse excavations.

In 1978, Brady and Bray[14] presented the displacement continuity method and Hocking[15] and Wardle and Crotty[16] used it in combination with the conventional boundary element method to analyse problems involving slip and discontinuity. Beer and Meek[17–19] also reported several major contributions, including combination of the boundary and finite element methods for mining application. Venturini and Brebbia[20] demonstrated how the technique can be used to simulate multilayer materials, with particular reference to thin layers for which spatial interface conditions have been considered. Rudolphi[21] has implemented the BEM using quadratic elements for zoned, two-dimensional bodies including discontinuous stress components.

Nowadays, the BEM is used as a powerful method to solve many mining and rock mechanics problems such as elastic and inelastic stress analysis of homogeneous and inhomogeneous regions, elastostatic, elastodynamic, elastoplastic, viscoplastic, creep, large-deformation and time-dependent behaviour of rock masses, fracture, groundwater and even heat transfer analysis for two- and three-dimensional regions. The boundary element reference book published by Mackerle and Brebbia[22] has a bibliography of most papers and references of BEM up to 1988.

NON-LINEAR DEFORMATION FAULT MODEL

The Barton–Bandis model describes the non-linear deformation of a joint with a path-dependent coupling of shear stress, τ, shear displacement, V_x, normal stress, σ_n, closure, V_z, Joint Roughness Coefficient (JRC), Joint Compressive Strength (JCS), peak shear displacement, V_{xp}, and maximum closure, V_{zm}. It also accounts for the mobilization of shear strength of fault using the mobilized joint roughness coefficient. Bandis *et al.*[23] described the complete normal stress versus closure relation of joint in terms of the initial normal stiffness, K_{ni}, and maximum closure. Their equation for the normal stiffness, K_n, is as follows:

$$K_n = \frac{K_{ni}}{(1 - V_z/V_{zm})^2} \tag{1}$$

Barton and Bakhtar[23] analysed a large number of shear test results reported in the literature and suggested the following equation for the peak shear stiffness, K_{xp}:

$$K_{xp} = \frac{\tau_p}{V_{xp}} \tag{2}$$

where the peak shear strength, τ_p, is obtained from

$$\tau_p = \sigma_n \tan\left[\mathrm{JRC}\log_{10}\left(\frac{\mathrm{JCS}}{|\sigma_n|}\right) + \phi_r\right] \tag{3}$$

Barton *et al.*[25] modified equation (3) to take into account the stress dependency of the shear strength. The stress–displacement history of a roack discotinuity is considered by using the mobilized joint roughness coefficient, JRC_m. The mobilized shear failure condition, τ_m, is given by

$$\tau_m = \sigma_n \tan\left[\mathrm{JRC}\log_{10}\left(\frac{\mathrm{JCS}}{|\sigma_n|}\right) + \phi_r\right] \tag{4}$$

BOUNDARY ELEMENT FORMULATION

Boundary element methods have generally developed in two parallel directions which are indirect and direct boundary element methods. The former method is further divided into two methods which are the Fictitious Stress (FS) method and the Displacement Discontinuity (DD) method. Problems of discontinuous rock mass can be analysed using a combination of FS and DD methods. In this paper, the FS method is used to model the boundary of the opening and the DD method is used for the simulation of discontinuities such as faults and bedding planes.

Figure 2 presents an example of an underground opening intersected by a fault. Boundary element modelling treats the opening boundary by M Fictitious Stress (FS) elements and fault by $N - M$ Displacement Discontinuity (DD) elements, whereby N is the total number of boundary elements.

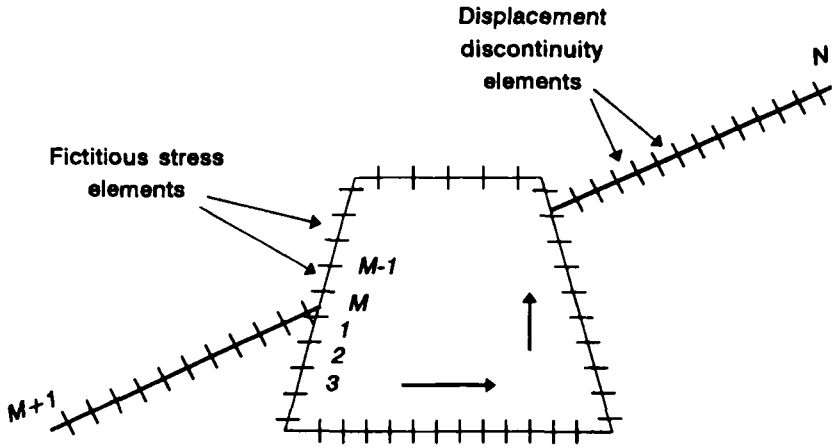

Figure 2. Boundary element modelling of an underground opening intersected by a fault

ALGORITHM FOR NON-LINEAR ANALYSIS

The non-linear analysis employs an incremental-iterative technique. The creation of an underground excavation is made by incrementally relaxing the boundary tractions applied to the FS elements. Iteration is performed within each load increment to assure numerical stability of the solution and a convergence criterion is used to terminate the iteration process. The size of each load step is determined by dividing the initial boundary tractions $(\sigma_s^i)_0$ and $(\sigma_n^i)_0$ into L equal segments. Thus, the boundary tractions applied in the kth load step are

$$(\sigma_s^i)_0^k = \frac{k}{L}(\sigma_s^i)_0$$

$$(\sigma_n^i)_0^k = \frac{k}{L}(\sigma_n^i)_0, \quad k = 1, L \tag{5}$$

The DD elements $M + 1 \leqslant i \leqslant N$ follow the Barton–Bandis model to determine the shear stress–slip relation along a fault.

Equilibrium of the system after each load increment step is achieved by iteration.[26] The parameter which controls the iteration is the convergence of the unknown vector $\{X\}_k^i$. The convergence of the vector $\{X\}_k^i$ in iteration j of load increment k is checked using the following criterion:

$$\frac{\| X_i \|_k^j - \| X_i \|_k^{j-1}}{\| X_i \|_k^j} \leqslant \varepsilon \tag{6}$$

Iteration at a load step is continued until the tolerance (ε) is less than 0·01. This condition helps prevent numerical instability of the solution. It is assumed that $\| X_i \|^{j-1} = 0{\cdot}0$ for the first iteration ($j = 1$). The norm $\| X_i \|$ is given by

$$\| X_i \| = \sqrt{X_1^2 + X_2^2 + X_3^2 + \cdots + X_n^2} \tag{7}$$

MODIFICATION OF K_n AND K_s FOR THE BARTON–BANDIS DEFORMATION MODEL

The model accounts for the non-linear deformation of fault. In each step, the normal and shear stiffnesses are modified based on the normal and shear displacements of that step. Figure 3 illustrates the non-linear behaviour of discontinuities through the rock mass.

The normal stress vs. closure is described by a hyperbolic function. The normal stiffness in the kth step for the ith DD element is updated using the current value of the normal displacement ($X_n^{i(k)}$) as follows:

$$K_n^i = \frac{K_{ni}^i}{(1 - X_n^{i(k)}/V_{zm}^i)} \tag{8}$$

where, for the ith DD element, K_n^i is the current normal stiffness, K_{ni}^i is the initial normal stiffness and V_{zm}^i is the maximum closure.

The maximum closure, V_{zm}^i, and the initial normal stiffness, K_n^i, are constant input data. When $X_n^{i(k)} \geqslant 0{\cdot}9\ V_{zm}^i$ the value of normal stiffness is kept constant and it has the same value as $X_n^{i(k)} = 0{\cdot}9\ V_{zm}^i$ which gives $K_n^i = 100\ K_{ni}^i$.

When yielding is detected in the DD elements, first the value of K_n is obtained from equation (8) and then it is reduced by a factor λ to account for the presence of yield. This factor is obtained from an experimental relation as follows:[25]

$$\lambda = 2 + \frac{\mathrm{JRC}^i\,\mathrm{JCS}^i\sigma_n^i}{2500} \tag{9}$$

The shear stiffness K_s^i is modified based on the value of shear displacement ($X_s^{i(k)}$). A review of a large number of shear tests is reported in the literature (650 data points from 35 references) by Barton and Bakhtar.[24] Based on these data, a model for the deformation of the fault was recommended which assumes that the behaviour of the fault is elastic when the value of the shear displacement is less than or equal to 0·3 times the maximum shear displacement. If the value of

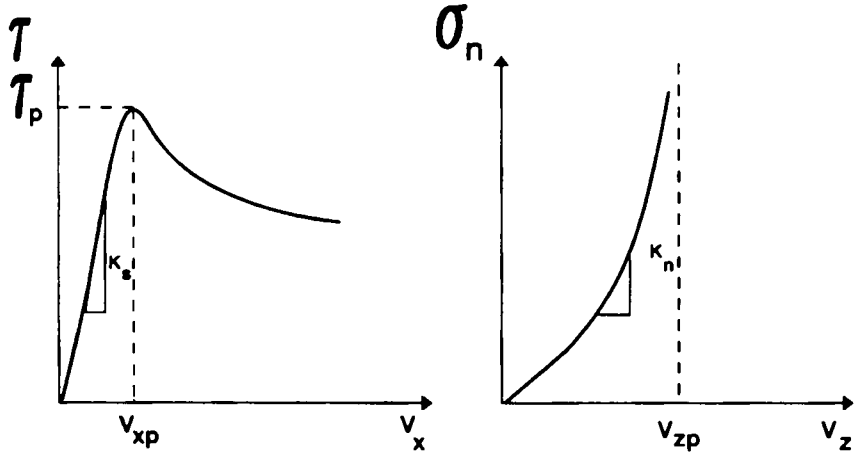

Figure 3. Non-linear behaviour of discontinuities in rock mass

$X_s^{i(k)} \leqslant 0{\cdot}3\ V_{xp}^i$, then the shear stiffness is modified as follows:

$$(K_s^i)^k = \left| \frac{(\tau_r^i)^k}{0{\cdot}3 V_{xp}^i} \right| \tag{10}$$

where $(\tau_r^i)^k$ is the residual shear stress of the ith DD element for the kth step. This is because during the elastic behaviour of shear stiffness, JRC_m is equal to zero. Therefore, the residual shear strength is obtained from

$$(\tau_r^i)^k = (\sigma_n^i)^k \tan(\varphi_r^i) \tag{11}$$

Now, considering equation (11), equation (10) can be written as

$$(K_s^i)^k = \left| \frac{(\sigma_n^i)^k \tan(\varphi_r^i)}{0{\cdot}3 V_{xp}^i} \right| \tag{12}$$

where the residual friction angle, φ_r^i, and peak shear displacement, V_{xp}^i, are constant input parameters. If the shear displacement $X_s^{i(k)} > 0{\cdot}3 V_{xp}^i$ then the shear stiffness is modified as follows:

$$(K_s^i)^k = \left| \frac{(\tau_m^i)^k}{X_s^{i(k)}} \right| \tag{13}$$

Now, considering equation (4), equation (13) can be written as follows:

$$(K_s^i)^k = \left| \frac{(\sigma_n^i)^k \tan(JRC_m^i \log(JCS^i/|(\sigma_n^i)^k|) + \varphi_r^i)}{X_s^{i(k)}} \right| \tag{14}$$

When a joint separation mode is detected in DD elements (i.e. tensile stress), both K_n and K_s are set equal to zero.

BARTON–BANDIS YIELD CRITERIA

The shear behaviour of the fault is considered based on the mobilization of joint roughness coefficient, JRC_m, during the shear movement of the fault. The mobilized joint roughness coefficient, JRC_m^i, of the kth step for the ith DD element is determined using the shear displacement component, $X_s^{i(k)}$. Figure 4 illustrates the behaviour of rough and smooth joints. As can be seen, the shear behaviour of smooth joints can be considered elastoplastic, whereas that of rough joints is elastoplastic followed by joint softening and residual strength behaviour. Joints are classified according to the magnitude of their peak joint roughness coefficient JRC_p: if $JRC_p \leqslant 5$, a joint is considered smooth; otherwise it is considered rough.

The developed boundary element model applies to both joint types. For purposes of illustration, the shear stress–displacement model suggested by Barton *et al.*[25] for rough joints is used. This is shown in Figure 5. Both shear stress and displacement are normalized, and hence the model is non-dimensional. Given the shear displacement component in a DD element, the model is used to obtain the mobilized joint roughness coefficient JRC_m^i. Given the normal stress $(\sigma_n^i)^k$ in the kth load step, the mobilized shear strength, τ_m^i, is calculated as follows:

$$(\tau_m^i)^k = (\sigma_n^i)^k \tan\left(JRC_m^i \log\left(\frac{JCS^i}{|(\sigma_n^i)^k|} \right) + \varphi_r^i \right) \tag{15}$$

The joint compressive strength, JCS, and residual friction angle, φ_r, are constant input data. The value of JCS is obtained from the Schmidt hammer test.[27]

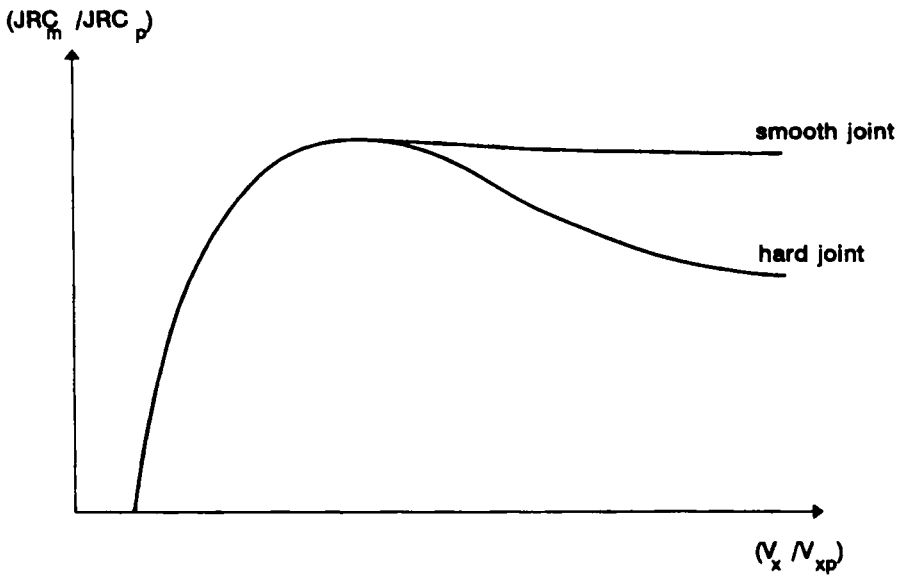

Figure 4. Shear deformation behaviour for smooth (JRC $\leqslant$ 5) and rough (JRC > 5) joints

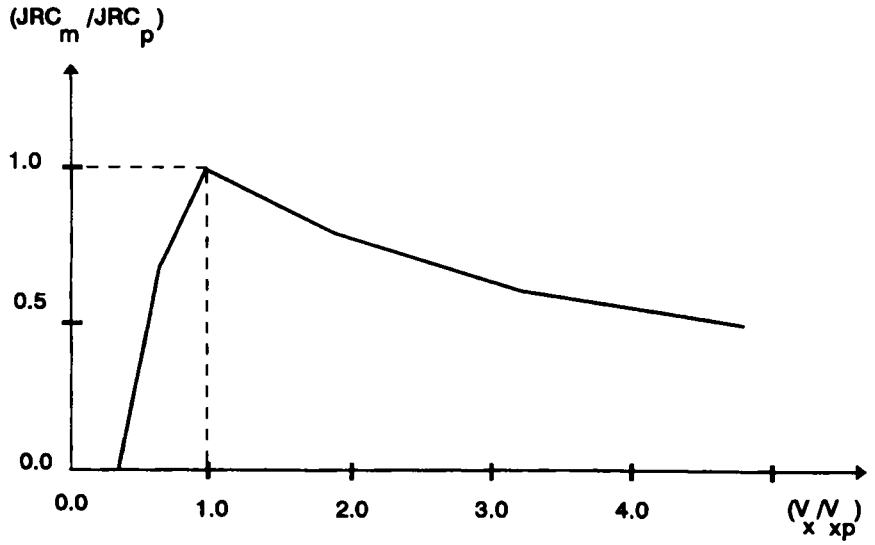

Figure 5. Dimensionless shear stress–displacement model

For each DD element, the maximum shear stress, τ_m, is compared with the applied shear stress, σ_s. If $\sigma_s \geqslant \tau_m$, it means that the DD element is yielding. But if $\sigma_s < \tau_m$, then it might be one of two cases: (1) the DD element has yielded in a previous step, or (2) the joint is in the elastic range and no modification is needed for the behaviour of the DD element.

NUMERICAL EXAMPLE

Crouch and Starfield[28] analysed a problem of a rectangular excavation located beneath a horizontal fault. The geometry of the problem is shown in Figure 6. The data that they used were as follows: Young's modulus of elasticity = 10,000 MPa, Poisson's ratio = 0·2, horizontal initial stress = 2·5 MPa, vertical initial stress = 5·0 MPa.

A Mohr–Coulomb fault model was assumed with cohesion (c) = 0 and angle of friction (φ) = 30°. The fault normal and shear stiffnesses are constant with normal stiffness (K_n) = 10^5 MPa/m and shear stiffness (K_s) = 10^5 MPa/m.

Due to symmetry about the y-axis, only half of the problem can be modelled. Half of the boundary of the excavation was modelled with 60 FS elements while 30 DD elements were used to discretize the fault.

The model was used to solve the same problem based on the Mohr–Coulomb peak strength model with constant joint stiffnesses, K_n and K_s. The technique of the solution is based on incremental relaxation of boundary tractions in 10 steps. Figure 7 shows the behaviour of three DD elements as the boundary tractions transit from one increment to the next. The DD elements are nos. 10, 15 and 20, respectively. The results obtained from the numerical model are identical to those reported by Crouch and Starfield.[28]

COMPARISON OF TWO JOINT MODELS

There is an important difference between classical Mohr–Coulomb and Barton–Bandis models. For the Mohr–Coulomb model, yielding of the joint is determined only by the comparison of the applied shear stress and the maximum shear stress. For the Barton–Bandis model, yielding of the joint is determined in two steps. The first step involves the comparison of the applied shear stress and the mobilized limit shear stress (or mobilized shear strength). Secondly, a comparison of joint shear displacement and maximum elastic shear displacement (0·3 V_{xp}) is made (when the shear

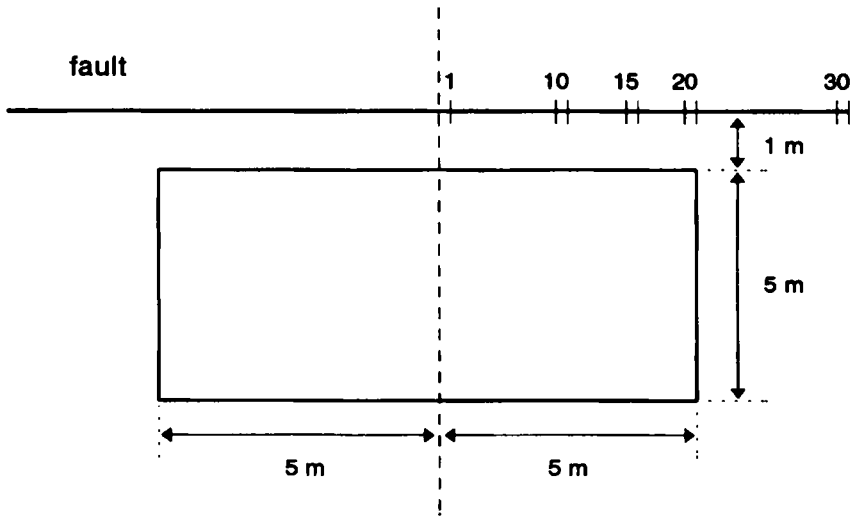

Figure 6. Geometry of the problem of a room underneath a horizontal fault

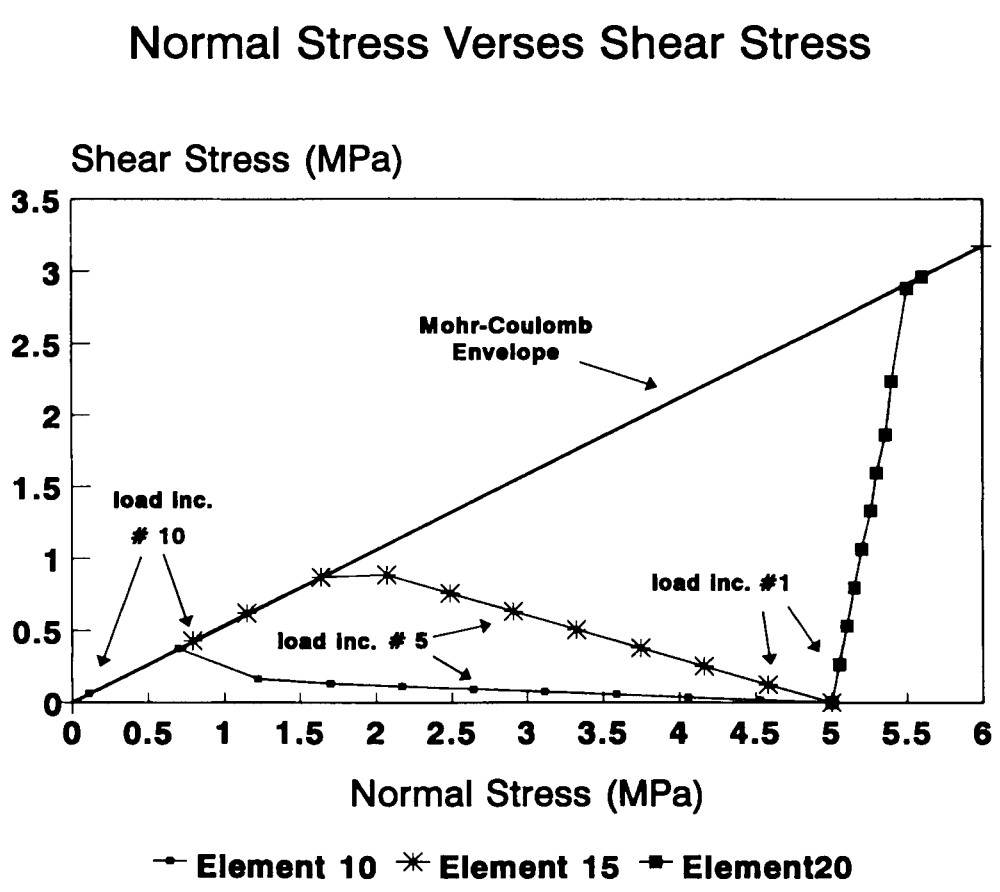

Figure 7. Behaviour of the DD element 10, 15 and 20 through load increments 1–10

displacement, V_x, is more than $0{\cdot}3V_{xp}$, the joint begins to yield). The latter one controls the hardening–softening–residual behaviour of the joint.

A geomechanical problem is examined using the two different joint models, namely Barton–Bandis and Mohr–Coulomb, for the purpose of comparison of model responses.[26] This mining problem represents an underground mine stope located 740 m below the surface and is intersected by an inclined fault. Figure 8 shows the geometry and dimensions of the stope and intersecting fault. The modelled domain is 70 m in the x-direction and 60 m in the y-direction. The rock mass has a unit weight of 0·027 MN/m^2 with a Young's modulus of elasticity of 50 GPa and a Poisson's ratio of 0·20. Also, the ratio of horizontal to vertical *in situ* stresses is 1·5.

The *in situ* stresses are linearly varying with depth below the surface. *In situ* stresses at the point of origin ($x = 0$, $y = 0$) are:

$$\text{vertical initial stress} = (\sigma_y)_0 = \gamma h = 740 \times 0{\cdot}027 = 20 \text{ MPa}$$

$$\text{horizontal initial stress} = (\sigma_x)_0 = 20 \times 1{\cdot}5 = 30 \text{ MPa}$$

The vertical and horizontal initial stresses for each DD and FS element are varied and are related to the depth of each element (h) below the surface.

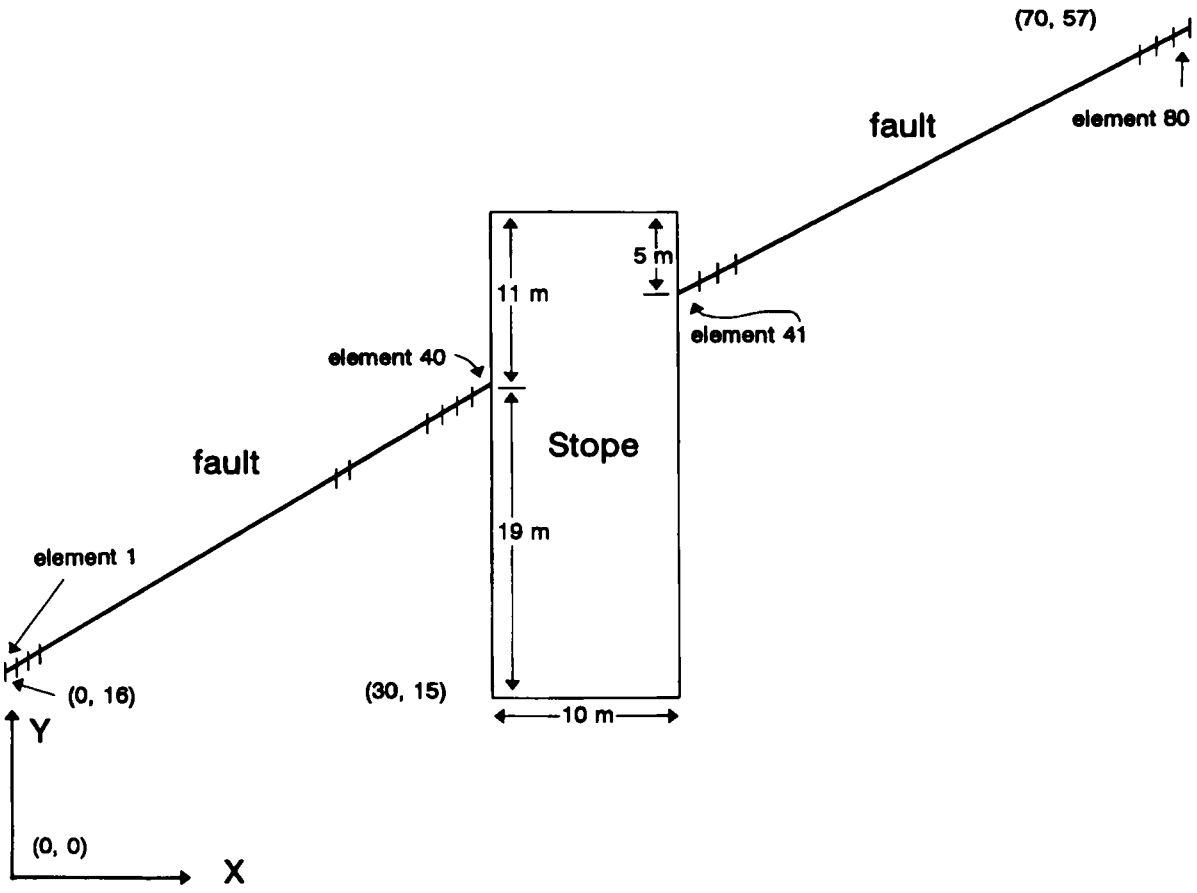

Figure 8. Modelling of a rectangular stope intersected by an inclined fault

Table I. Barton–Bandis fault model parameters — problem in Figure 8

c	φ_b	K_{ni} (MPa/m)	K_{si} (MPa/m)	V_{zm} (mm)	V_{xp} (mm)	JRC	JCS (MPa)
0	30	10,000	3000	5	5	15	60

The stope is modelled by 60 FS elements and the fault by 80 DD elements. For the fault, elements 1–40 are on the left side of the stope and 41–80 are on the right side as shown in Figure 8.

The problem is first analysed using the Barton–Bandis model. The fault characteristics for the Barton–Bandis model are presented in Table I.

The model, then, is used to solve the same problem using the Mohr–Coulomb model with constant fault stiffness. The following fault parameters are assumed:

$$c = 0, \quad \varphi = 30°, \quad K_s = 3000 \text{ MPa/m}, \quad K_n = 10{,}00 \text{ MPa/m}.$$

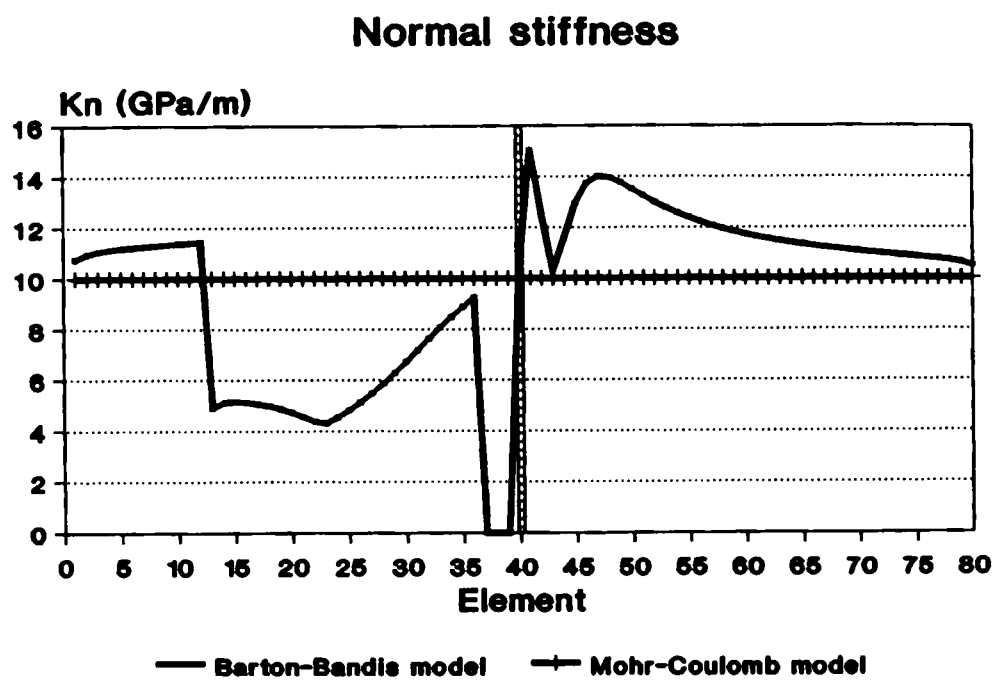

Figure 9. Comparison of normal stiffness after load step 10 between Barton–Bandis and Mohr–Coulomb models

The normal and shear stiffnesses of all joint elements, after 10 steps, are presented in Figures 9 and 10, respectively. Figure 9 shows that K_n is constant for the Mohr–Coulomb joint model but is varied for the Barton–Bandis model based on the last deformation of each element. Also it shows that the value of K_n is generally higher on the right side of the stope (elements 41–80), which is due to the higher normal stress on the fault on the right side which reduces the possibility of yielding in that zone of the fault. The drop of K_n for the elements form 14 onwards indicates the presence of yielding in those elements. Figure 10 again shows a constant K_s for the Mohr–Coulomb fault model but a varying one for the Barton–Bandis model and also a higher value on the right side of the stope.

The dimensions normal and shear displacements of all joint elements, after 10 steps, are presented in Figures 11 and 12, respectively. The sign convention for normal displacement, V_z, is negative for closure and positive for opening. The phenomena of both closure and opening occur under compressive normal stress. Separation is a case which occurs only when a tensile normal stress is calculated along the fault ($K_n = 0$, $K_s = 0$). Figure 11 shows almost the same result of V_z/V_{zm} for both models, The results of the Barton–Bandis model may be considered more realistic (for example, a drop in the value of V_z for element 14 because of yielding). From Figure 12, it is seen that whereas the absolute values of shear displacements of the fault on the right side of the stope (elements 41–80) are the same for both models, they are higher on the left side for the Barton–Bandis model.

Figure 13 presents the friction angle (φ) of all DD joints elements after the load step number 10. Figure 13 shows that the friction angle of fault on the right side of the stope is almost the same for both models (because of linear behaviour), whereas on the left side it is constant for the Mohr–Coulomb model but variable for the Barton–Bandis model (because of varying deformations of each element during the load increments).

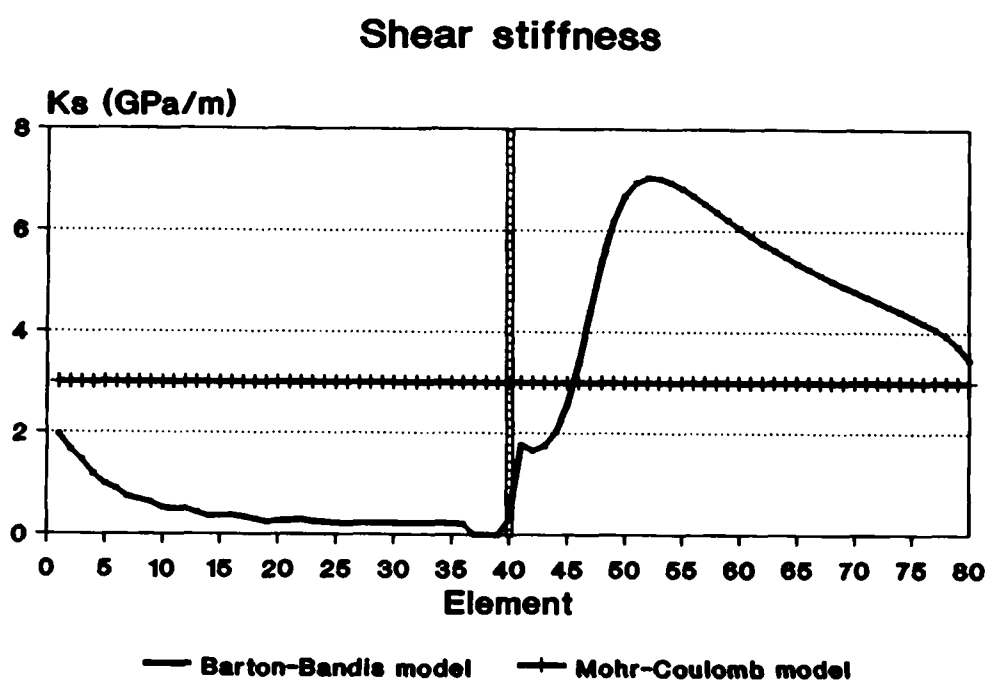

Figure 10. Comparison of shear stiffness after load step 10 between Barton–Bandis and Mohr–Coulomb models

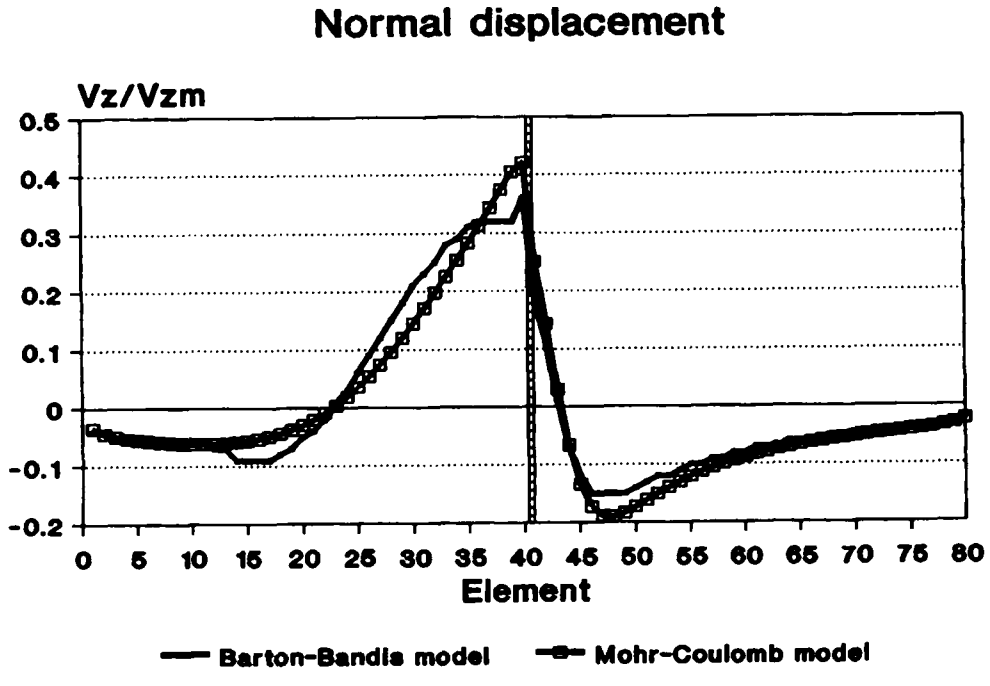

Figure 11. Comparison of the ratio V_z/V_{zm} after load step 10 between Barton–Bandis and Mohr–Coulomb models

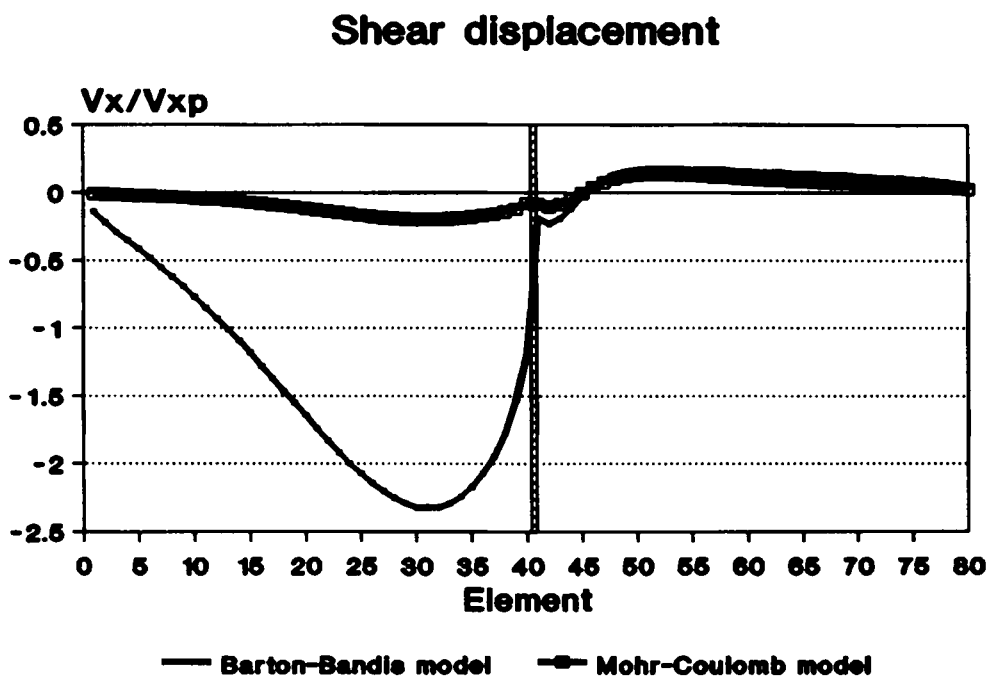

Figure 12. Comparison of the ratio V_x/V_{xp} after load step 10 between Barton–Bandis and Mohr–Coulomb models

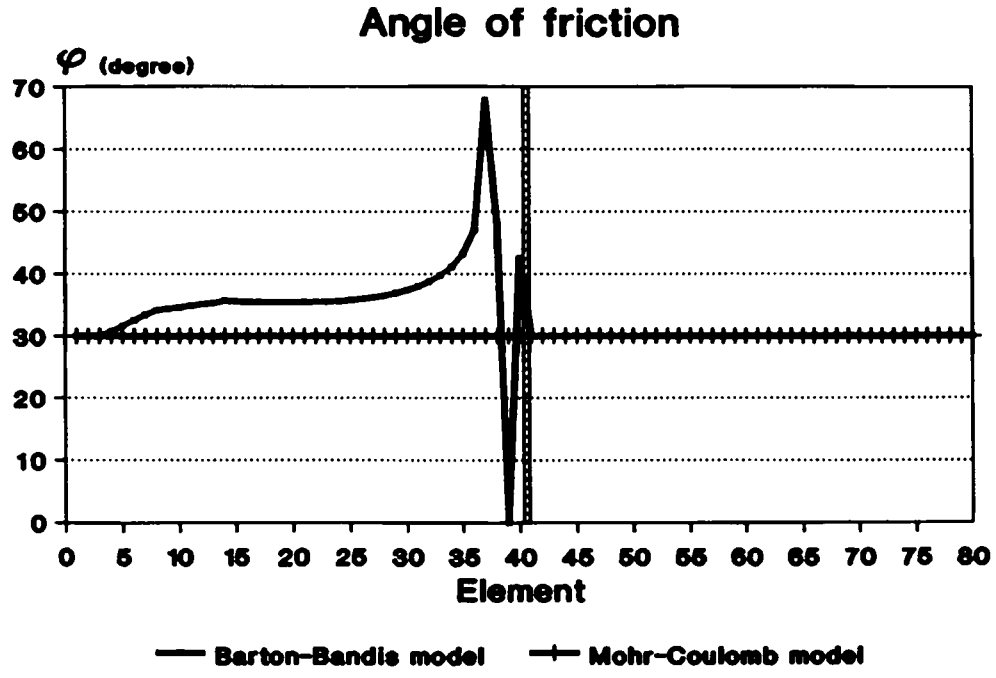

Figure 13. Comparison of friction angle (φ) after load step 10 between Barton–Bandis and Mohr–Coulomb models

CASE STUDY

The developed numerical model has been used to conduct a case study with actual data from a Canadian underground hard rock mine. Ore is extracted using the blasthole stoping method. The nominal dimensions of the stope are 60 m high by 15 m wide with lengths ranging from 30 to 45 m. Figure 14 shows a plan view of the case study at a depth of 700 m below the surface. A fault passes through the foot wall and is thought to play a major role in the stability of this level of the mine. The stope mining sequences are marked A, B, C and D from hanging wall to foot wall.

The numerical model is used to examine the behaviour of the fault when mining activity takes place close to the fault (mining proceeds from stope A to stope D). The values of the *in situ* stresses from the field at this mining level are

$$\sigma_1 = 52 \text{ MPa}, \quad \sigma_2 = 39 \text{ MPa}$$

The *in situ* stresses are assumed to be constant because the problem domain is a horizontal section of the mine. The mechanical properties of rock mass used for input data are as follows:

$$E = 67 \text{ GPa}, \quad \nu = 0{\cdot}28$$

The characteristics of the fault are determined from the field and are used for input data. These are presented in Table II.

Various types of consolidated backfill are used at this mine. The presence of backfill in a stope was simulated by applying a constant normal stress along the boundary of stopes. Based on the available information, it was decided that the constant normal stress be 2 MPa.

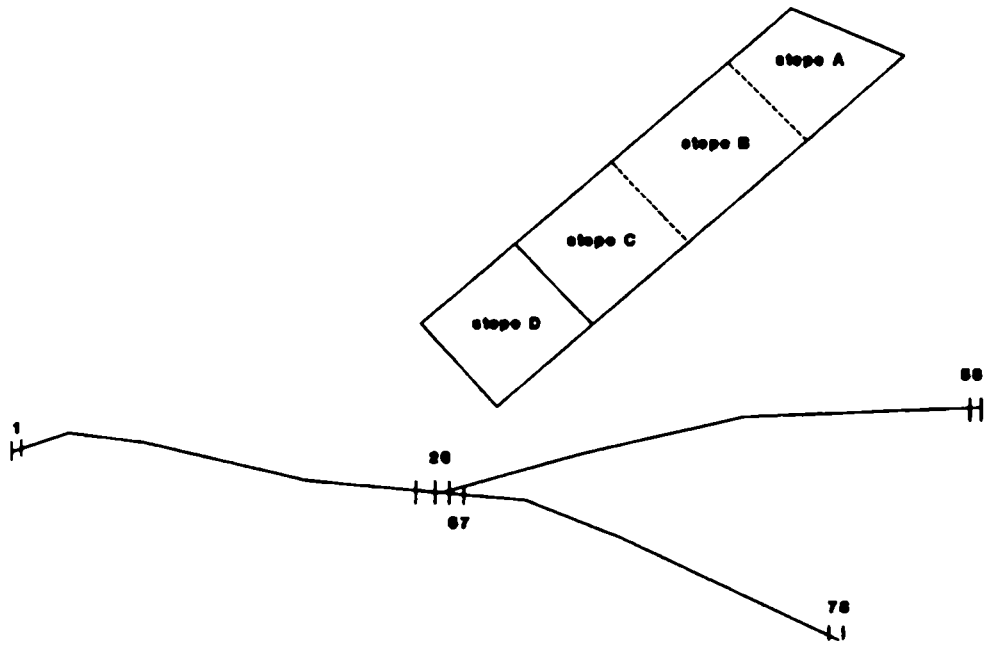

Figure 14. A plan view and mining sequences of the case study

Table II. Barton–Bandis fault model parameters — problem in Figure 14

K_{ni} (MPa/m)	K_{si} (MPa/m)	V_{zm} (mm)	V_{xp} (mm)	JRC	JCS (MPa)	φ_r (deg.)	σ_c (MPa)
13,000	3500	9	9	11	46	33	160

Table III. Numerical models constructed for the case study

Model	Explanation
1	Stope A is mined out
2	Stope A is backfilled and B is mined out
3	Stopes A and B are backfilled and C is mined out
4	Stopes A, B and C are backfilled and D is mined out

Table IV. The number of elements and run times of different models

Model	Fault (DD)	Stope (FS)	Iteration	Run time (min)
1	78	30	20	33
2	78	50	20	49
3	78	65	20	69
4	78	82	20	92

A total of four numerical models were constructed to help examine the fault behaviour after each stope had been excavated/filled. Table III describes the modelled scenarios. The number of FS and DD elements as well as model run times are recorded in Table IV.

The results of the four mining sequences with backfill simulation have been presented in much greater detail elsewhere.[26] Some of the results are given herein.

Figure 15 shows the variation of distribution of shear displacement along the fault. Shear displacement is increased in three sections significantly (elements 6–26, elements 32–46 and elements 57–65). The zone of elements 32–56 has high movement (between 2 and 12 times of the peak shear displacement) which should be considered for support design. Figure 16 shows the variation of the distribution of normal displacements along the major fault.

Unfortunately, there was no field instrumentation to measure the stress and displacement of rock mass. But a comparison of the results showed good agreement with what was observed at the mine. Considerable seismic activity has been recorded in the same area of the fault which was predicted to have significant movement by the numerical model (the zone of elements 32–56). In a site visit of the mine, it was observed that failure of the rock mass occurred in the same zone that was predicted by the numerical model.

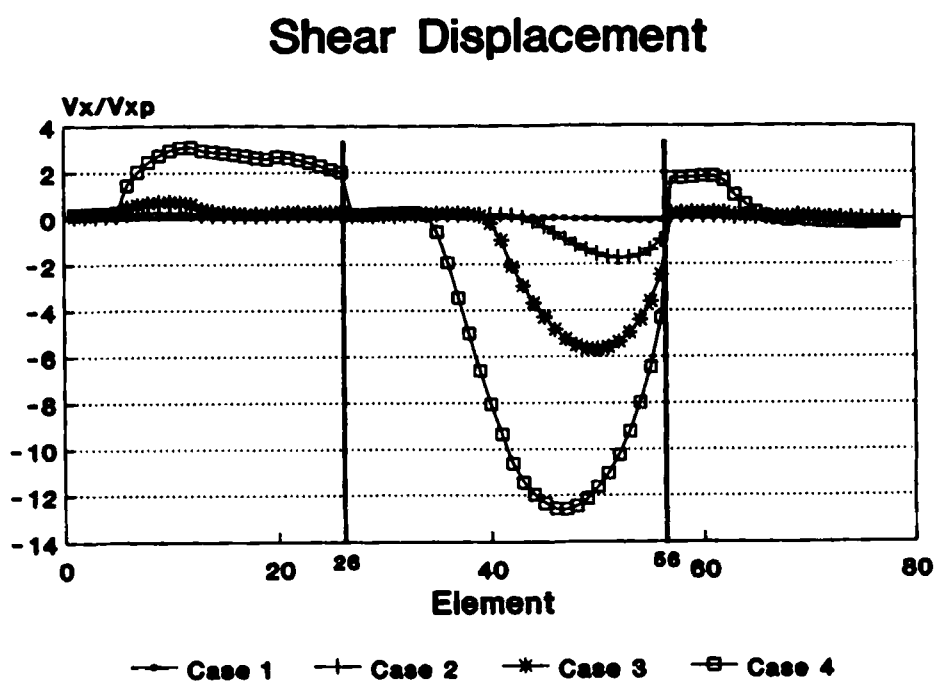

Figure 15. Shear displacement distribution along the fault — case study

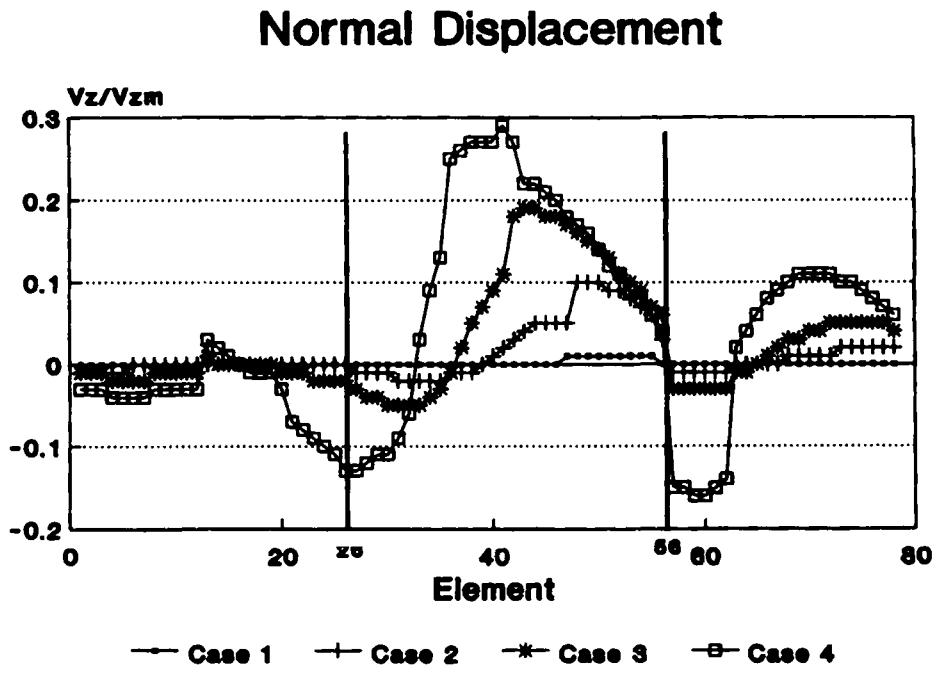

Figure 16. Normal displacement distribution along the fault — case study

CONCLUSIONS

An indirect boundary element method involving fictitious stress and displacement discontinuity techniques is adopted to develop a new non-linear model capable of simulating two-dimensional sections of underground rock excavations in the neighbourhood of faults. Both deformation and peak strength non-linear, joint models of Barton–Bandis were incorporated in the numerical model. A comparison of the Barton–Bandis model with the classical Mohr–Coulomb model has revealed the benefits to be gained for adopting the former model for the stimulation of a more realistic behaviour of faults. The case study presented in this paper demonstrates that the developed model can be utilized to shed light on the stability and fault–slip behaviour around underground mine openings.

ACKNOWLEDGEMENT

This work has been funded by a research grant from the Natural Science and Engineering Research Council of Canada (NSERC). The authors are grateful for NSERC's financial support.

REFERENCES

1. R. E. Goodman, R. L. Taylor and T. Brekke, 'A model for the mechanics of jointed rocks', *J. Soil Mech. Found. Eng.*, **94**, 637–659 (1968).
2. R. E. Goodman, *Methods of Geological Engineering*, West, St. Paul, 1976.
3. M. Fortin, G. Archambault, M. Aubertin and D. E. Gill, 'An algorithm for predicting the effect of a variable normal stiffness on shear strength of discontinuities', *Proc. 15th Canadian Rock Mechanics Symp.*, Toronto, 1988.
4. M. Fortin, D. E. Gill, M. Aubertin, B. Ladanyi and G. Archambault, 'Stimulating the effect of a variable normal stiffness on shear behaviour of discontinuties', *Mechanics of Jointed and Faulted Rocks*, Balkema, Vienna, 1990.
5. S. Saeb and B. Amadei, 'Modelling joint response under constant or variable normal stiffness boundary conditions', *Int. J Rock Mech. Min. Sci. Geomech. Abstr.* **27**, 213–217 (1990).
6. R. E. Goodman and W. Boyle, 'Non-linear analysis for calculating the support of a rock block with dilatant joint faces', *34th Geomechanics Colloquy*, Salzburg, Austria, 1985.
7. S. Saeb and B. Amadei, 'Modelling rock joint under shear and normal loading', *Int. J. Rock Mech. Min. Sci. Geomech. Abstr.*, **29**, 267–278 (1992).
8. M. D. G. Salamon, 'Elastic analysis of displacements and stresses induced by the mining of seam or reef deposites — part I', *J. South African Inst. Mining Metallurgy*, **64**, 129–149 (1963).
9. M. D. G. Salamon, 'Elastic analysis of displacements and stresses induced by the mining of seam or reef deposits — part II', *J. South African Inst. Mining Metallurgy*, **64**, 197–218 (1964).
10. M. D. G. Salamon, 'Elastic analysis of displacements and stresses induced by the mining of seam or reef deposits — part III', *J. South African Inst. Mining Metallurgy*, **64**, 468–500 (1964).
11. M. D. G. Salamon, 'Elastic analysis of displacements and stresses induced by the mining of seam or reef deposites — parts IV', *J. South African Inst. Mining Metallurgy*, **65**, 319–338 (1964).
12. A. M. Starfield and S. L. Crouch, 'Elastic analysis of single seam extraction', in H. R. Hardy Jr. and R. Stefhanko (eds), ASCE, New York, 1973, pp. 421–439.
13. F. H. Deist, 'A new digital method for three dimensional stress analysis in elastic media', *Rock Mech.*, **5**, 189–202 (1973).
14. B. H. G. Brady and J. W. Bray, 'The boundary element method for determining stress and displacements around long openings in a triaxial stress field', *Int. J. Rock Mech. Min. Sci. Geomech. Abstr.*, **15**, 21–28 (1978).
15. G. Hocking, 'Stress analysis of underground excavations incorporating slip and separation along discontinuities', in C. A. Brebbia (ed.), *Recent Advances in Boundary Element Methods*, Pentech Press, London, 1978, pp. 195–214.
16. L. J. Wardle and J. M. Crotty, 'Two dimensional boundary integral equation analysis for non-homogeneous mining applications', in C. A. Brebbia (ed.), *Recent Advances in Boundary Element Methods*, Pentech Press, London, 1978, pp. 233–251.
17. G. Beer, and J. L. Meek, 'Coupled finite element–boundary element analysis of infinite domain problems', *Proc. Int. Conf. on Numerical Methods for Coupled Problems*, Pineridge Press, Swansea, Wales, 1981.
18. G. Beer and J. L. Meek, 'Efficient analysis in geomechanics', in A. A. Eisenstein (ed.), *Proc. 4th Int. Conf. on Numerical Methods in Geomechanics*, Balkema, Rotterdam, 1982, Vol. 1, pp. 5–13.
19. G. Beer and J. L. Meek, 'Applications in mining', in *Topics in Boundary Elements Research*, Springer, Berlin, 1984, Vol. 1, Chap. 8.

20. W. S. Venturini and C. A. Brebbia, 'Applications in geomechanics', in *Topics in Boundary Element Research*, Springer, Berlin, 1984, Vol. 1, Chap. 7.
21. T. J. Rudolphi, 'An implementation of the boundary element method for zoned media with stress discontinuties', *Int. j. numer. methods eng.*, **19**, 1–15 (1983).
22. J. Mackerle and C. A. Brebbia, *The Boundary Element Reference Book*, Computational Mechanics Publications, Springer, Berlin, 1988.
23. S. C. Bandis, A. C. Lumsden and N. R. Barton, 'Fundamentals of rock joint deformation', *Int. J. Rock Mech. Min. Sci. Geomech. Abstr.* **20**, 249–268 (1983).
24. N. R. Barton and K. Bakhtar, 'Rock joint and description and modelling for the hydrothermomechanical design of nuclear waste repositories', CANMET, Mining Research Laboratories, Ottawa, 1983.
25. N. R. Barton, S. Bandis and K. Bakhtar, 'Strength, deformation and conductivity coupling of rock joints', *Int. J. Rock Mech. Min. Sci. Geomech. Abstr.*, **22**, 121–140 (1985).
26. K. Fotoohi, 'Nonlinear boundary element analysis of rock mass with discontinuities', *Ph.D. Thesis*, McGill University, Montreal, Canada, 1994.
27. E. Hoek and J. Bray, *Rock Slope Engineering*, 2nd edn, The Institution of Mining and Metallurgy, London, 1977.
28. S. L. Crouch and A. M. Starfield, *Boundary Element Methods in Solid Mechanics*, 1st edn, George Allen & Unwin, London, 1983.